Non-universality of halo profiles and implications for dark matter experiments

Reed, D S ; Koushiappas, S M ; Gao, L

DOI: https://doi.org/10.1111/j.1365-2966.2011.18930.x

Monthly Notices
of the
ROYAL ASTRONOMICAL SOCIETY

Mon. Not. R. Astron. Soc. **415,** 3177–3188 (2011) doi:10.1111/j.1365-2966.2011.18930.x

Non-universality of halo profiles and implications for dark matter experiments

Darren S. Reed,[1⋆] Savvas M. Koushiappas[2] and Liang Gao[3,4]

[1]*Institute for Theoretical Physics, University of Zürich, Winterthurerstrasse 190, CH-8057 Zürich, Switzerland*
[2]*Department of Physics, Brown University, 182 Hope St., Providence, RI 02912, USA*
[3]*National Astronomical Observationaries, Chinese Academy of Science, Beijing 100012, China*
[4]*Institute for Computational Cosmology, Department of Physics, University of Durham, South Road, Durham DH1 3LE*

Accepted 2011 April 15. Received 2011 April 15; in original form 2010 August 9

ABSTRACT

We explore the cosmological halo-to-halo scatter of the distribution of mass within dark matter haloes utilizing a well-resolved statistical sample of clusters from the cosmological Millennium Simulation. We find that at any radius, the spherically averaged dark matter density of a halo (corresponding to the 'smooth component') and its logarithmic slope are well described by a Gaussian probability distribution. At small radii (within the scale radius), the density distribution is fully determined by the measured Gaussian distribution in halo concentrations. The variance in the radial distribution of mass in dark matter haloes is important for the interpretation of direct and indirect dark matter detection efforts. The scatter in mass profiles imparts approximately a 25 per cent cosmological uncertainty in the dark matter density at the Solar neighbourhood and a factor of $\sim$3 uncertainty in the expected Galactic dark matter annihilation flux. The aggregate effect of halo-to-halo profile scatter leads to a small (few per cent) enhancement in dark matter annihilation background if the Gaussian concentration distribution holds for all halo masses versus a 10 per cent enhancement under the assumption of a lognormal concentration distribution. The Gaussian nature of the cluster profile scatter implies that the technique of 'stacking' haloes to improve signal-to-noise ratio should not suffer from bias.

Key words: galaxies: haloes – cosmology: theory – dark matter.

1 INTRODUCTION

Overwhelming evidence indicates that most of the mass in the Universe is composed of dark matter. In the concordance Lambda cold dark matter (ΛCDM) cosmological model, structure formation is dominated by the gravitational evolution of dark matter. At the present epoch, most of the mass has been assembled into self-bound haloes, which are hosts to the galaxies, clusters and groups that are observed. Although the exact nature of dark matter is unknown, theoretically motivated extensions to the standard model of particle physics suggest cold dark matter candidates which were in thermal equilibrium in the early Universe and interact only weakly with baryonic matter.

Weakly interacting massive particles (WIMPs) are ideal dark matter candidates as they arise naturally in many extensions of the standard model of particle physics. The strength of their interactions can mimic the physical behaviour of the dark matter (weak as well as gravitational) inferred from a broad range of observations. WIMP dark matter candidates have a small but non-zero cross-section for self-annihilation (Jungman, Kamionkowski & Griest 1996). Indirect detection experiments look for the by-products of this annihilation, typically in the form of high-energy photons, neutrinos and positrons, as well as low-energy antiprotons (see Jungman et al. 1996; Bertone, Hooper & Silk 2005).

In recent years, halo structure has been widely explored using cosmological numerical simulations. Pioneering work by Navarro, Frenk & White (1996, 1997; NFW hereafter) used numerical simulations to show that the spherically averaged radial density profile of dark matter haloes is approximately 'universal'. However, NFW and later Jing (2000) and Bullock et al. (2001) noted significant variations in the profile between different haloes, in that some are better fitted by steeper (higher concentration) profile forms than others. These variations were shown to be correlated with halo formation time (e.g. Wechsler et al. 2002). Upon close inspection, the profile of any individual halo cannot be described by any particular smooth functional form (e.g. Jing 2000; Reed et al. 2005; Gao & White 2006; Knollmann, Power & Knebe 2008; Lukić et al. 2009). In this sense, the halo mass profile is not truly 'universal'. Thus, due to this fundamentally non-smooth nature of the radial mass distribution of

⋆E-mail: reed@physik.uzh.ch

haloes, functional forms do not provide a complete and accurate description of the halo density.

In this paper, we quantify the mean and scatter of the halo radial mass distribution without the a priori assumption of a smooth functional form. We use a large sample of haloes extracted from the 'Millennium' cosmological numerical simulation, whose combination of large volume and fine mass resolution are ideal for studying statistical variations in halo mass profiles. Our approach begins with an empirical non-parametric measure of the distribution function of halo densities, allowing us to include the effects of halo-to-halo and intrahalo non-universality in addition to effects relating to scatter in halo concentrations. We focus on small radii where the 'smooth' dark matter component dominates the mass distribution; here, self-bound satellite 'subhaloes' are deficient because of efficient tidal stripping before reaching small radii (Springel et al. 2008). This allows us to quantify the cosmological scatter in the smooth component of the dark matter density. We apply our results to several cosmological applications, including direct and indirect experimental efforts of dark matter detection.

Annihilation of dark matter scales as the square of the number density of particles, and thus any detected annihilation signal will be sensitive to the precise distribution of dark matter. Past work focused on using extremely high resolution simulations of individual dark matter haloes of Galactic mass to estimate annihilation luminosities for particular dark matter candidates (Kuhlen, Diemand & Madau 2008; Springel et al. 2008). These impressive numerical simulations were able to quantify the level at which substructure contributes to the annihilation signal, as well as get a glimpse of the phase-space structure of the Milky Way halo at the Solar neighbourhood. However, halo-to-halo variations in the radial mass profile implies a 'cosmological' uncertainty in the predicted annihilation rate in haloes, which is of course in addition to the uncertainties related to the mass, cross-section, and other properties of the dark matter particle.

Dark matter annihilation in haloes produces a cosmological background whose strength depends upon the numbers of haloes throughout the history of the Universe and their density profiles (e.g. Ullio et al. 2002; Zavala, Springel & Boylan-Kolchin 2010). When integrated over all haloes, a scatter in halo density profiles implies a boost of the annihilation background with respect to the case where all haloes follow a universal profile without scatter (e.g. Ullio et al. 2002). The strength of the annihilation background will thus be sensitive to both the average *and* the scatter in halo dark matter profiles. Inferring the dark matter particle mass and cross-section from a background annihilation signal will thus require separating out the integrated effects of cosmological scatter.

In addition, even within the Milky Way, interpretation of both direct and indirect dark matter detection efforts requires an understanding of the intrinsic variance in halo profiles. The cosmological uncertainty in the local dark matter density at the solar radius is essential in the interpretation of a detection (or lack of) in direct detection experiments. In particular, knowledge of the intrahalo scatter in density with radius is needed to evaluate results of direct (local) dark matter detection efforts in the context of indirect (non-local) detection experiments focused on the Galactic Centre or elsewhere. Thus, both direct and indirect dark matter detection efforts face the challenge of disentangling the influences of cosmological haloes from the properties of the dark matter particle.

In this paper, we use a large number of cosmological haloes to quantify the cosmological variance in halo densities, and to assess the level at which the distribution of halo densities affects the interpretation of dark matter direct and indirect detection experiments. In Section 2, we review the general characteristics of dark matter halo mass distribution, and we give an overview of the cosmological simulations that we use in Section 3. We present our analysis of the mass distribution and its scatter within haloes in the simulation in Section 4, showing that the distribution of halo concentrations yields an accurate description of the measured scatter of the smooth component of dark matter within haloes. We apply our findings to experimental searches of dark matter in Section 5; we discuss limitations of our work (Section 6), followed by a brief conclusion (Section 7).

2 THE DARK MATTER HALO PROFILE

As a baseline reference for examining the cosmological scatter of halo density profiles, it is convenient to parametrize the density profile by a spherically averaged functional form. Recent works favour the Einasto (1965) profile form as a description of cosmological haloes (Navarro et al. 2004; Gao et al. 2008; Hayashi & White 2008). In this case, the logarithmic slope of the density is a simple power law:

$$\frac{\mathrm{d}\ln\rho}{\mathrm{d}\ln r} = -2\left(\frac{r}{r_{-2}}\right)^{\alpha}. \tag{1}$$

The 'scale radius', $r = r_{-2}$, has a density slope of -2, and defines the halo concentration as

$$c_{\rm vir} = \frac{r_{vir}}{r_{-2}}, \quad \text{or} \quad c_{200} = \frac{r_{200}}{r_{-2}}, \tag{2}$$

where in the first definition, $r_{\rm vir}$ is the virial radius of the halo, defined as a sphere of 95.4 times critical density (Eke, Cole & Frenk 1996), while in the second definition, r_{200} is the radius where the enclosed density is 200 times the critical density of the Universe. The parameter α in equation (1) varies weakly with mass and redshift. On average $\alpha = 0.19$, for $z = 0$ clusters over the mass range that we explore (as shown in Gao et al. 2008). Density is given by

$$\rho(r) = \rho_{-2}\exp\left\{-\frac{2}{\alpha}\left[\left(\frac{r}{r_{-2}}\right)^{\alpha} - 1\right]\right\}. \tag{3}$$

The normalization of the profile is obtained from requiring that the mass of the halo is $M = \int_0^{R_{200}} 4\pi\rho(r)r^2\mathrm{d}r$, thus

$$\rho_{-2} = \frac{2^{3/\alpha}c_{200}^3 M}{4\pi\,\mathrm{e}^{2/\alpha}\alpha^{(3-\alpha)/\alpha}R_{200}^3\left[\Gamma\left(\frac{3}{\alpha}\right) - \Gamma\left(\frac{3}{\alpha}, \frac{2c_{200}^{\alpha}}{\alpha}\right)\right]}. \tag{4}$$

Here, $\Gamma(x)$ and $\Gamma(x, y)$ are the Gamma, and Incomplete Gamma functions respectively.

3 SIMULATIONS AND HALO CATALOGUE

We utilize the gravity-only N-body particle *Millennium Simulation* of Springel et al. (2005). This simulation evolves 2160^3 particles in a periodic box of $500h^{-1}$Mpc using the gravity solver code LGADGET2 (Springel et al. 2005), a modified version of the publicly available GADGET2 (Springel 2005). Particle mass is $8.6 \times 10^8\, h^{-1}\,\mathrm{M}_{\odot}$. The cosmological parameters used are $\Omega_{\rm m} = 0.25$, $\Omega_{\Lambda} = 0.75$, hubble constant $h = 0.73$, $\Omega_{\rm b} = 0.045$, $n = 1$, with power spectrum normalization $\sigma_8 = 0.9$. The matter power spectrum used to create initial conditions is produced using CMBFAST (Seljak & Zaldarriaga 1996).

For this study, it is important to use as large a statistical sample of haloes as possible. In addition, these haloes must be resolved in the innermost regions in which we are interested. We thus consider

all haloes with more than 10^5 particles, corresponding to $M_{\rm vir} \geq 8.6 \times 10^{13}\,h^{-1}\,{\rm M}_\odot$. This results in 3501 haloes. The density profiles for these haloes are resolved down to ∼1–2 per cent $r_{\rm vir}$, based on convergence tests in Moore et al. (1998), Power et al. (2003) and Reed et al. (2005) for haloes with similar numbers of particles.

We define haloes and their centres using the same procedure as was done in Neto et al. (2007) and Gao et al. (2008). Haloes are identified initially using *friends-of-friends* with linking length of 0.2 times the mean interparticle spacing. Haloes are centred on the location of the deepest potential of the main subhalo. Halo mass is then determined by a sphere of 95.4 times critical density ($M_{\rm vir}$), and additionally by a sphere of 200 times critical density (M_{200}). We determine a spherically averaged logarithmically binned density profile for each halo.

4 COSMOLOGICAL VARIATIONS IN THE HALO PROFILE

In this section we discuss the cosmological variance in the properties that describe the profile of dark matter haloes.

4.1 Halo concentrations

Halo concentrations have been shown to have significant halo-to-halo scatter, with a median that decreases with increasing mass and redshift (e.g. Bullock et al. 2001; Neto et al. 2007; Duffy et al. 2008; Gao et al. 2008; Maccio, Dutton & van den Bosch 2008). Early work suggested that the distribution of halo concentrations is lognormal (Jing 2000; Bullock et al. 2001). However, larger samples of higher resolution haloes reveal significant departures from a lognormal scatter, primarily due to a tail of low concentrations inferred from 'unrelaxed' haloes (Neto et al. 2007; Maccio et al. 2008), which tend to conform poorly to smooth functional fits (Lukić et al. 2009). In fact, the distribution of halo concentrations is very well described by a simple Gaussian, as noted by Lukić et al. (2009), when all (relaxed and unrelaxed) haloes are considered. In Fig. 1 we show the concentration probability distribution function (PDF) from our full sample. We find that a Gaussian description of concentrations is a better fit than a lognormal distribution to the haloes in our sample. More complicated functional descriptions of halo concentrations such as that suggested by Neto et al. (2007) or by Maccio et al. (2008) appear unnecessary to describe our data (which consists of the high mass halo subset of the haloes of Neto et al. 2007 and Gao et al. 2008).

In estimating halo concentrations, we consider both the Einasto profile (equations 1–4) and the NFW profile (NFW 1996, 1997):

$$\rho = \frac{4\rho_{-2}}{(r/r_{-2})(1 + r/r_{-2})^2}. \quad (5)$$

A concentration defined by the Einasto profile is, in principle, equivalent to that defined by the NFW profile, both having a scale radius at r_{-2}. However, because simulation haloes tend to better match the Einasto form, which is steeper than NFW at the smallest radii, a concentration inferred from the NFW form can be biased high or low, depending on the range of radii used in fitting (see Gao et al. 2008). We find that although the Einasto profile produces a better fit to stacked haloes, the distribution of concentrations is modestly narrower when fit according to an NFW profile (see Fig. 1), with approximately the same mean value ($c_{200,\rm NFW} = 4.55$ versus $c_{200,\rm Einasto} = 4.50$). The Einasto distribution remains wider, whether or not the Einasto parameter α is fixed or allowed to float as a free parameter in the fit. For this reason (and also for convenience), we determine halo concentrations by fitting the NFW profile (equation 5) in the remainder of this paper. We stress that the shape of the Einasto-fit distribution of concentrations is nearly identical to that of the NFW-fit concentration PDF; the only difference is that the Einasto-fit concentration PDF is slightly wider (∼10 per cent) Gaussian. Profiles are fit to logarithmic radial bins over a range of

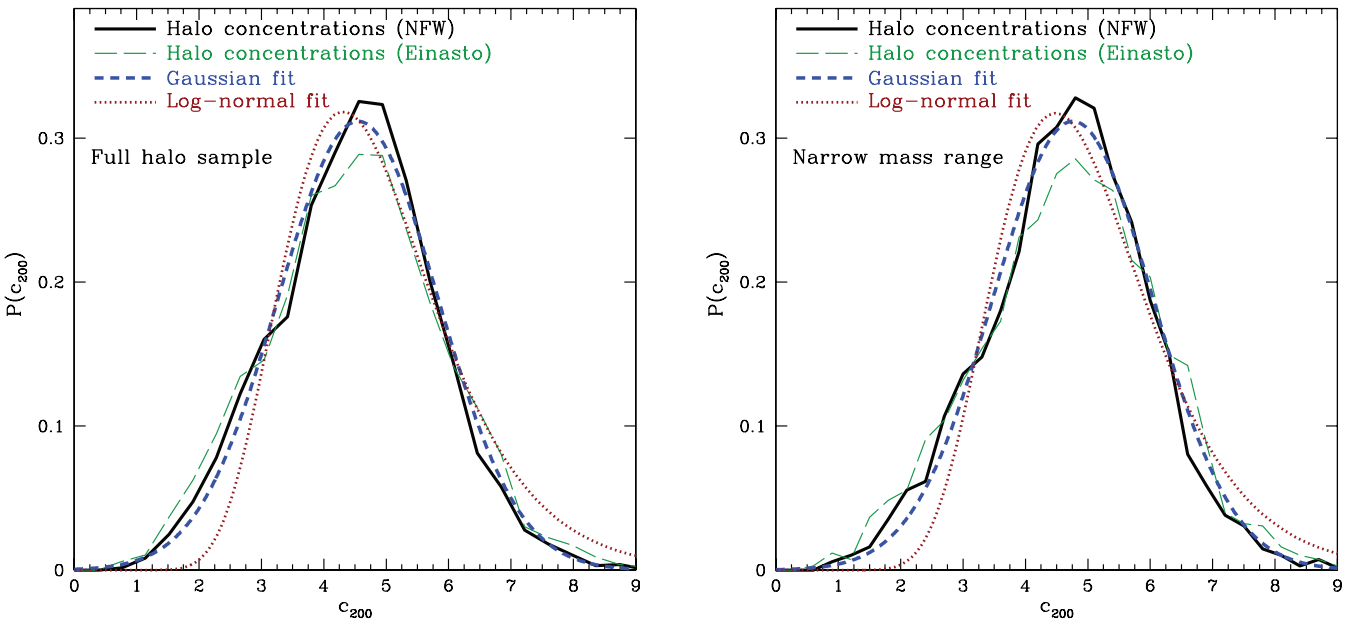

Figure 1. Left-hand panel: the PDF of concentrations for the 3501 haloes with $M \geq 8.6 \times 10^{13}\,h^{-1}\,{\rm M}_\odot$ shown against best-fitting Gaussian with a mean $\langle c \rangle = 4.55$, and standard deviation $\sigma_c = 1.28$. This provides a better match than the best-fitting lognormal distribution with a mean $\langle \log_{10} c \rangle = 0.669$ and a standard deviation in $\log c$ of $\sigma_{\log c} = 0.121$. Concentration fits made to the NFW profile produce a modestly narrower distribution, even though the Einasto profile is overall a better description of the halo mass distribution. Right-hand panel: the distribution of concentrations in a narrow virial mass range of $8.6 \times 10^{13} \leq [M/h^{-1}\,{\rm M}_\odot] \leq 1.7 \times 10^{14}$ (2276 haloes). The shape of the concentration PDF remains Gaussian.

$0.05 - 1r_{200}$ with normalization set by the mass contained within r_{200}.

We have confirmed also that fixing the density normalization instead of allowing it to float as a fit parameter has no significant effect upon the derived concentrations. As a further test, we show that the relatively wide range in halo masses for our full sample does not affect the shape of the distribution of concentrations. With a narrower sample mass range of 2times in mass ($8.6 \times 10^{13} \leq [M_{\rm vir}/h^{-1}\,{\rm M}_{\odot}] \leq 1.7\times10^{14}$), a Gaussian concentration distribution is still preferred over lognormal (right-hand panel of Fig. 1). The similar shape for the narrower mass range is not surprising because the mass dependence on mean halo concentration is relatively weak; and more importantly, this shows that the shape of the concentration distribution is not sensitive to our choice of the width of the mass range for the halo sample used throughout the paper.

4.2 Halo densities

It is important to note that the Einasto profile has been found to fit haloes well for a 'stacked' ensemble (e.g. Hayashi & White 2008; Gao et al. 2008). However, the presence of substructure and other peculiarities implies that any particular halo profile tends to have significant variations from this mean smooth function.

In the left-hand panel of Fig. 2, we show this scatter in the density profile for 100 random haloes. The spread in densities due to different concentrations is also apparent. The right-hand panel of Fig. 2 shows that there is very large scatter in the logarithmic slope of the density profile, plotted here versus r/r_{-2}. This representation removes differences that arise due to concentration. The increased scatter in density slopes at outer radii is independent of mass within our sample (i.e. similar behaviour is seen for the 100 least massive haloes in the sample); large radii scatter is likely enhanced by large substructures. The mean slope of the complete halo sample is well described by an Einasto profile, and is poorly matched by an NFW profile.

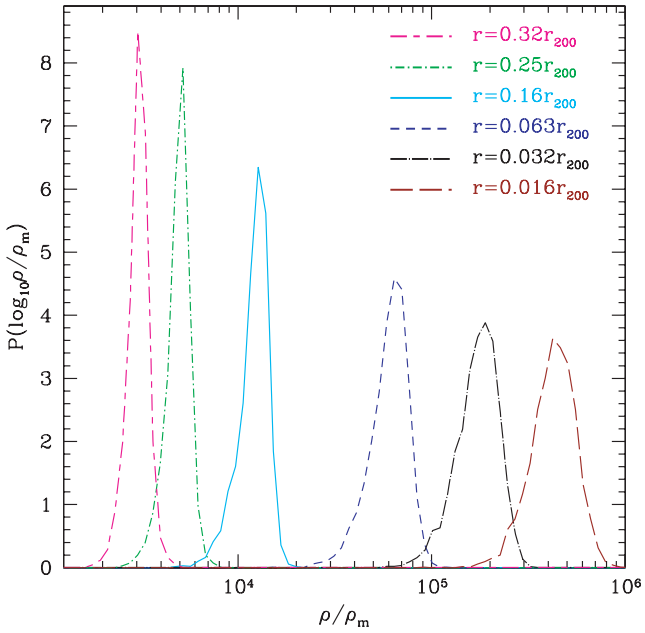

Figure 3. Halo-to-halo distribution in density at various radii relative to r_{200} in the full halo sample. Densities are plotted in units of mean density of the universe, $\rho_{\rm m}$.

In Fig. 3, we show the PDF of densities at various radii in spherically averaged shells from the halo sample. The width of the halo-to-halo scatter of density decreases towards larger radii. A possible explanation for this radial trend results from the fact that the central structure of the halo is assembled at higher redshifts than the outer parts of the halo (see e.g. Fukushige, Kawai & Makino 2004; Reed et al. 2005). If one assumes that halo density at a particular radius correlates with the mean density of the universe at the time of mass infall, then scatter in mass assembly redshift from halo to

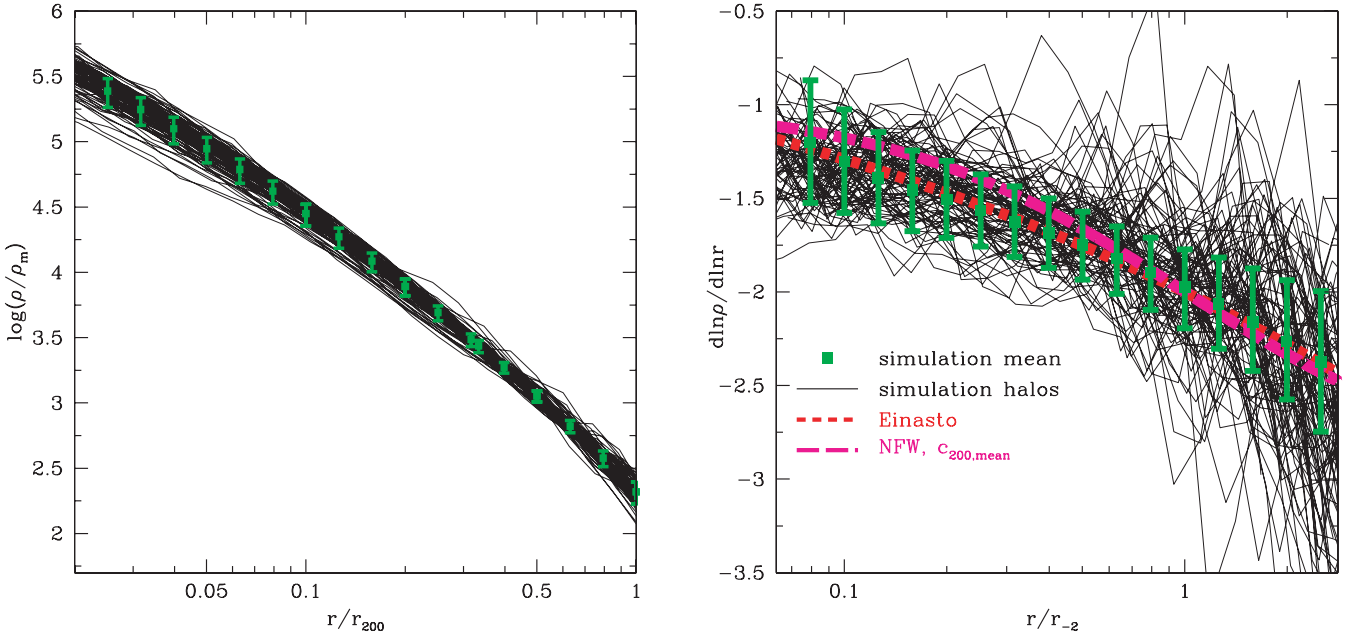

Figure 2. Left-hand panel: density profiles for 100 random haloes from the sample. Points with error bars denote the mean and the 1σ scatter of the distribution for the full halo sample. Right-hand panel: Logarithmic density slope for the 100 largest haloes. Slopes are normalized to the scale radius to remove the effect of scatter in halo concentrations. An Einasto profile with $\alpha = 0.19$ is a good match to the mean simulation slope.

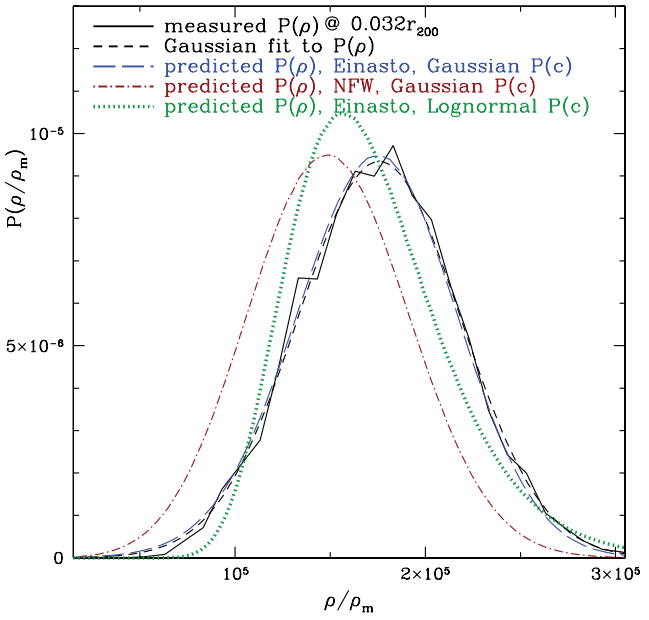

Figure 4. Measured density distribution at $0.032r_{200}$, as an example, versus density distribution predicted by a deterministic Einasto profile and a Gaussian concentration distribution of width $\sigma_{c200} = 1.28$, centred on $c_{200} = 4.55$ to match the measured values of our sample. Lognormal concentration prediction assumes the best fit to our sample of $\sigma_{\log 10c} = 0.121$ with median $c = 4.66$. Gaussian concentrations match the shape and peak position of the density distribution better than lognormal concentrations. Note that the concentration distribution for all curves comes from an NFW concentration fit (even when applied to the Einasto profile), which produces essentially equivalent concentrations to an Einasto fit (see Fig. 1 and Section 4.1); we use such NFW-derived concentrations here and hereafter.

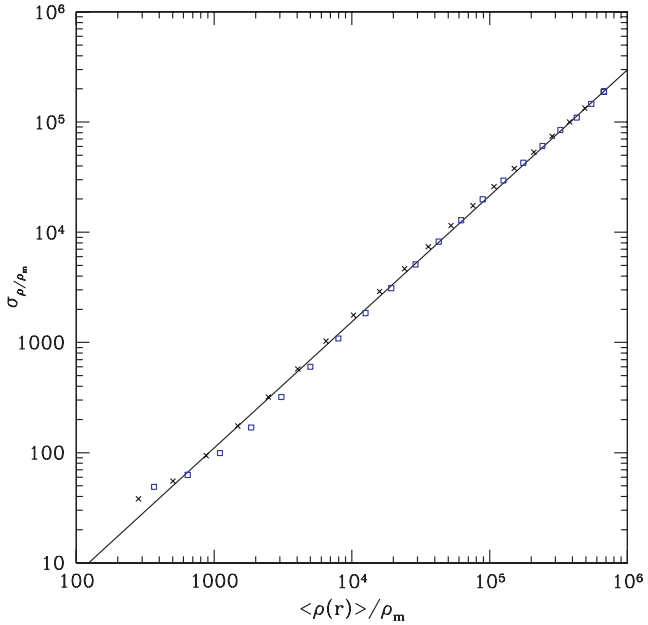

Figure 5. The width of the distribution of densities at various radii, σ_ρ, as determined by fitting a Gaussian, plotted as a function of mean density of our halo sample at each fitted radius for fixed $r/r_{\rm vir}$ (black crosses) and for fixed r/r_{200} (blue squares). The density distribution, $P(\rho)$, is well described by a Gaussian distribution at all radii. Line is a fit given by equation 6.

halo would yield density variations that would be larger nearer the centre due to the $(1+z)^3$ evolution of the mean matter density. Note that, at all radii, the width of the distribution is small compared to the statistical measurement uncertainty, which is estimated from Poisson counting of particles in radial bins.

The halo density PDF is well described by a Gaussian at each radius. As an example, in Fig. 4, we show the density distribution function at a radius of $r = 0.03r_{200}$. This scatter in densities is primarily due to the distribution in halo concentrations rather than intrahalo departures from a smooth functional form (i.e. 'bumps'). For small radii ($r \lesssim r_{-2}$), the Gaussian PDF of halo spherical shell densities is well matched by assuming that each halo is described by a deterministic Einasto radial density profile whose concentration is drawn from a Gaussian distribution (see Fig. 4). This implies that the distribution of halo concentrations fully determine the PDF of the smooth density component, and provides additional support that the form of the concentration PDF is Gaussian. More specifically, the effect of radial density 'bumps' within the halo cannot be larger than the effect of measurement uncertainty of individual halo concentrations. A lognormal concentration distribution is unable to reproduce the density distribution shape or peak. Unsurprisingly, an assumption of an NFW profile does not match the density peak, although it is able to produce the Gaussian shape and width.

At larger radii ($r \gtrsim r_{-2}$), the distribution remains Gaussian but is wider than implied by the distribution of concentrations, possibly due to increased scatter introduced from substructure or from a lower degree of relaxation in the outskirts of these recently formed cluster-size haloes. The distribution of densities in our data is described to (∼10 per cent) accuracy by the following function:

$$\log_{10}\sigma_\rho = 1.144\,\log_{10}\langle\rho\rangle - 1.389, \qquad (6)$$

where $\langle\rho\rangle$ and σ_ρ are found via a Gaussian fit to the densities measured from the halo sample at a given radius. The agreement between the fit and the simulation data, shown in Fig. 5, over more than three orders of magnitude in density is interesting. However, we do not advocate that this is a universal function; further work is required to determine whether this relation between density and its scatter remains valid for lower halo masses and different redshifts. The moderate flattening of σ_ρ at low density reflects the relative widening of the density PDF at large halo radii.

It is instructive to consider also the distribution of halo density profile slopes. In Fig. 6, we show the distribution of the logarithmic radial slope of the density at various radii. The PDF of $\mathrm{d}\ln\rho/\mathrm{d}\ln r$ is well described by a Gaussian distribution, except perhaps at large radii where substructure or other effects appear to result in wider than Gaussian tails. The mean of this distribution at each radius is consistent with the Einasto profiles with $\alpha = 0.19$. Note that the Einasto profile with fixed α implies zero scatter in the PDF of halo slopes. The radii in the right panel of Fig. 6 are chosen such that they should have identical logarithmic slopes, assuming the Einasto profile, for the mean halo concentration of 4.55.

For most radii, the width of the distribution of slopes is similar whether measured in terms of r_{-2} or in terms of r_{200}, apart from the innermost plotted radius. This is surprising because differences in halo concentrations should contribute to the spread in $\mathrm{d}\ln\rho/\mathrm{d}\ln r$ only at fixed r/r_{200}, and not at fixed r/r_{-2}, according to the Einasto (or NFW) self-similar profile form in which $\mathrm{d}\ln\rho/\mathrm{d}\ln(r/r_{-2})$ is independent of concentration. For this reason, we naively would have expected the spread in density slopes to be smaller at fixed r/r_{-2} than at fixed r/r_{200} (provided that r_{-2} is determined accurately). This suggests that intrahalo 'bumps' rather than halo concentration is the major contributor to scatter in the slope PDF. In fact, equation (1)

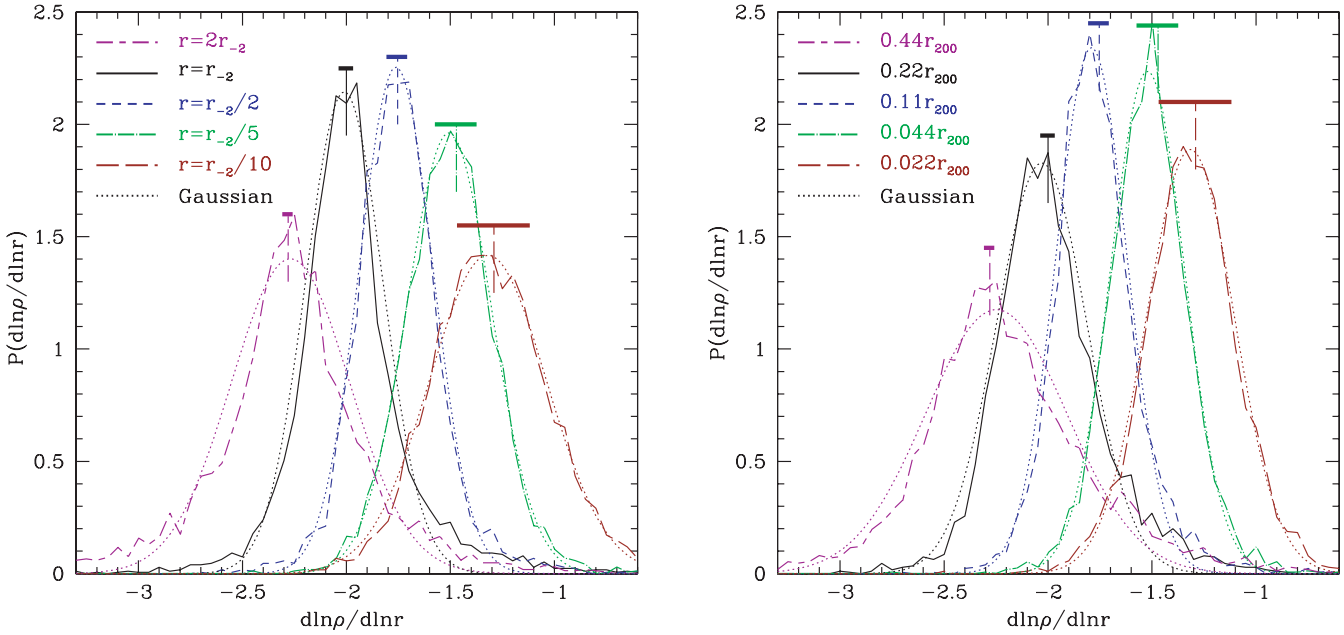

Figure 6. Distribution in halo slopes at various radii (solid lines) relative to the scale radius ($r_{-2} = r_{200}/c_{200}$) (left), and relative to r_{200} (right). Dotted curves are best-fitting Gaussians. Vertical lines denote the slope of the Einasto profile with $\alpha = 0.19$. In the right-hand panel, the Einasto profile slopes are shown for the mean halo concentration of 4.55. Slopes are reasonably fitted by a Gaussian with an average consistent with the Einasto profile and a width that is narrowest near r_{-2}. Again, these concentrations (i.e. r_{-2}) are estimated from an NFW profile fit, which is essentially equivalent to a direct Einasto fit. Horizontal lines indicate an estimate of the slope measurement uncertainty.

implies that the distribution in density slopes at fixed r/r_{200} due to the concentration distribution should be $\lesssim$0.1, which is much smaller than the actual spread which ranges from $0.17 < \sigma_{\mathrm{d\ln\rho/d\ln r}} < 0.34$ at the fixed r/r_{200} values shown.

At the smallest radius of $r_{-2}/10$, the slope distribution width is likely dominated by errors in the concentration measurement (left-hand panel). Presumably for this reason, the PDF of the slopes is narrower when considered with respect to r_{200} at the smallest radii. At each radius, we show an estimate of the uncertainty in the slope measurement, based on poisson noise from the average number of particles per radial bin. The slope uncertainty is significantly smaller than the measured PDF, except at the smallest plotted radius. Because numerical problems are most difficult to overcome at small radii, poisson uncertainty could underestimate the true error. We thus cannot rule out the possibility that the broadened PDF at small radii may have numerical origins. Indeed, increasing the minimum halo mass of the sample by a factor of 5 narrows the slope PDF at the smallest radii such that this effect is significantly smaller.

5 EFFECTS OF PROFILE SCATTER ON DARK MATTER ANNIHILATION

In this section we discuss the effect of the profile scatter on the expected signal in γ-rays (or other byproduct) from dark matter annihilation in haloes.

In general, the total γ-ray luminosity from a halo of mass M is given by the volume integral of the square of its mass distribution as

$$\mathcal{L} = \frac{\langle\sigma v\rangle}{M_\chi^2}\int_0^{R_v}\rho_{\mathrm{M}}^2(r)\mathrm{d}^3, \qquad (7)$$

where M_χ is the mass of the dark matter particle, and $\langle\sigma v\rangle$ is the thermal average of the annihilation cross-section. Particle physics enters through the mass of the dark matter particle, and through its total annihilation cross-section. As an example, in order to demonstrate the effects of density distributions on the annihilation flux, we consider a dark matter particle with mass $M_\chi = 400$ GeV, with a total annihilation rate to $b\bar{b}$ quarks given by $\langle\sigma v\rangle = 10^{-26}\,\mathrm{cm^3\,s^{-1}}$. We assume these values throughout the rest of this manuscript, and note that in general, the assumed dark matter particle properties affect the normalization of the results presented, and not the shape of the distributions.

The 'dark luminosity' of a halo is determined by the distribution of its mass (see equation 7). We assume that the *mean* distribution of dark matter in haloes is described by the Einasto profile, from equations (1)–(4). For the remainder of this section, we focus on the dark luminosity of the smooth component in a halo and thus we ignore the presence of substructure and any associated 'boost' that may contribute to the annihilation luminosity as defined in equation (7).

5.1 The flux distribution as a function of mass

We first confirm that we can capture the PDF of the local dark matter annihilation volume emissivity (in spherical shells). This is the quantity that will be integrated to compute total halo annihilation luminosity. In Fig. 7, we compare the measured distribution of normalized differential annihilation luminosity per logarithmic radial interval ($4\pi\rho^2(r)r^3$), shown here at $r = 0.032r_{200}$ as an example, with that from an Einasto profile (with $\alpha = 0.19$) with the mean concentration and Gaussian scatter of the halo sample (equation 7). We plot this distribution in units of mean density and r_{200} so that the quantity is independent of halo mass. The excellent agreement of measured and predicted differential annihilation luminosity implies that the concentration distribution with the assumption of an Einasto profile is sufficient to estimate localized (in radius) dark matter annihilation luminosity. However, we have yet to establish

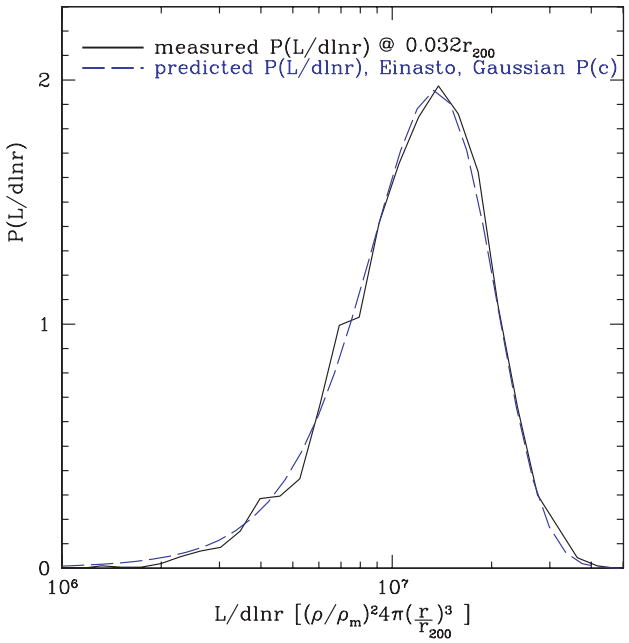

Figure 7. Normalized dark matter annihilation 'luminosity' per logarithmic radial interval ($4\pi\rho^2(r)r^3$) for the full halo sample. The prediction assumes an Einasto profile with a Gaussian concentration scatter, as in Fig. 4.

that the localized annihilation strength can be integrated to yield the correct halo annihilation luminosity. Correlations of density with radius could result in large scatter in annihilation luminosity from halo to halo. For example, haloes that happen to have enhanced density over some extended range below r_{-2}, where the annihilation rate is larger (albeit within a smaller volume), could have enhanced annihilation luminosity versus haloes with smoother profiles and similar concentrations. Although the results of Section 4 imply that intrahalo radial correlations are less important than the scatter in concentrations on local density, the ρ^2-dependence of annihilation could lead to a larger impact on halo annihilation rates.

In order to assess the origin of the scatter in halo annihilation luminosities and the contribution due to the scatter in concentrations, we compute the dark luminosity of each simulation halo, and compare with the expected luminosity given its measured concentration. We show in Fig. 8 the distribution of halo dark luminosities computed directly from the simulation halo density profile (left-hand panel) together with the prediction of the same quantity from an Einasto profile using the individually measured concentration of each halo (right-hand panel). We bin the data in mass, and determine the mean and 68 percentile of the distribution. The measured and predicted luminosities and 1σ scatter agree well; this suggests that *radial correlations* in density should not prevent accurate estimation of the *annihilation luminosity* of a halo.

Thus, the origin of the distribution of luminosities at each mass bin is the distribution in concentrations, which correlate with formation time, albeit with large scatter (see e.g. Neto et al. 2007). The correlation between concentration and annihilation luminosity can be modelled in the following manner for the smooth density component of dark matter haloes. The normalization of the profile is proportional to $\rho_{-2} \sim c_{200}^{\gamma}$, where $\gamma \sim 3$ for $c_{200} \gg 1$ and $r_{-2} \sim c_{200}^{-1}$. It follows that, roughly speaking, the luminosity scales as $L \sim \rho_{-2}^2 {r_{-2}}^3 \sim c_{200}^{2\gamma-3}$, leading to $L \sim c_{200}^3$ for $c_{200} \gg 1$, although for concentrations typical of our clusters $L \sim c_{200}^{1.5}$. Note that it is difficult to distinguish between the subtle differences between a Gaussian distribution of concentrations and a lognormal one from Fig. 8. In addition, we note that the mean of the luminosity distribution at each mass bin is roughly proportional to the mass of the halo. This is to be expected as the luminosity of a dark matter distribution that is described by a two-parameter profile (e.g., NFW, and/or Einasto) is $L \sim \rho_{-2}^2 {r_{-2}}^3 \sim M^{\beta}$, where $\beta \approx 1$ because the dependence of concentration on mass is relatively weak.

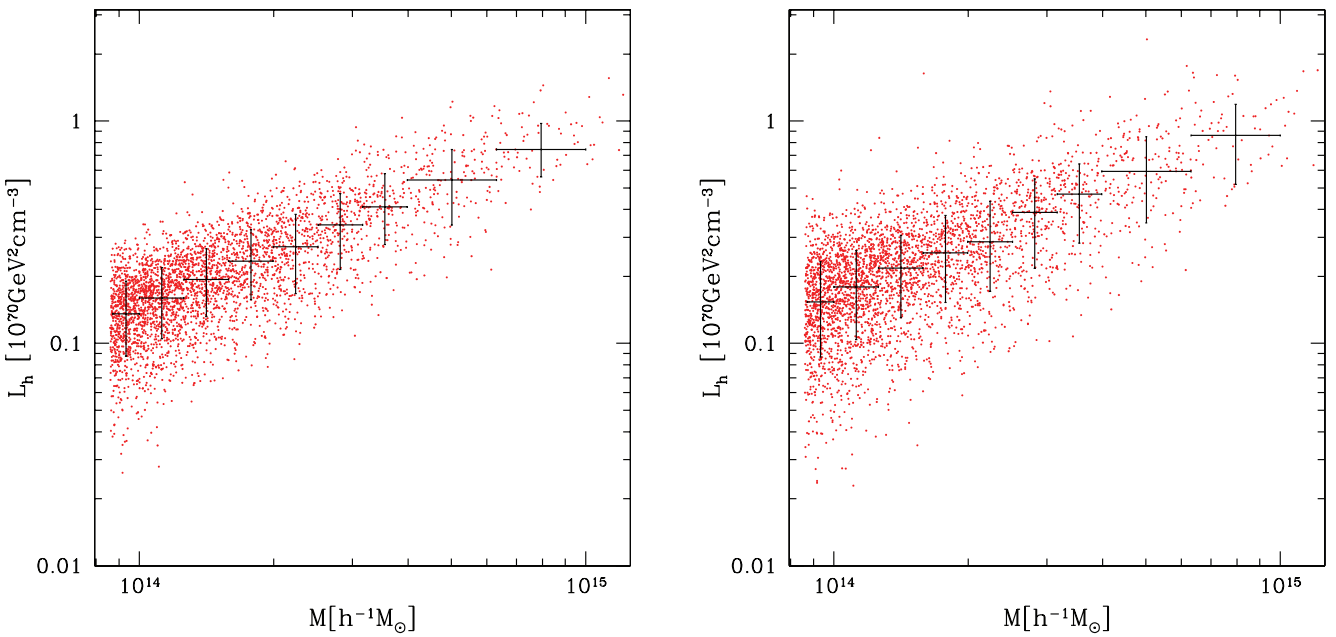

Figure 8. The inferred dark matter luminosities in units of 10^{70} GeV^2 cm^{-3}. Each dot represents a dark matter halo, while the vertical bars represent the 68 percentile of the distribution in each virial mass bin, whose width is denoted by the horizontal bars. Left-hand panel: luminosity computed directly from the density profile extracted from the simulation for each halo. Right-hand panel: expected luminosity computed from fitting a concentration to each halo and assuming an Einasto density profile.

5.2 Cosmological γ-ray background

We now consider the contribution of the scatter in densities to the cosmological γ-ray background: the annihilation flux integrated over all haloes at all masses and redshifts. We are interested in the effects of the non-universality of profiles to the expected γ-ray background. In Section 4.2, we showed for cluster haloes that the distribution in halo concentrations fully describes the distribution in halo densities (at small radii). This enables an accurate estimate of the distribution in dark matter annihilation luminosities (see Section 5.1). In order to estimate the dark matter annihilation background, we assume that this holds for haloes of all masses at all redshifts.

We compute the γ-ray background as

$$\frac{\mathrm{d}N_\gamma}{\mathrm{d}E\mathrm{d}A\mathrm{d}t\mathrm{d}\Omega} = \frac{1}{4\pi}\frac{c}{H_0}\int_0^\infty\int_{M_{\rm min}}^\infty \frac{\langle\sigma v\rangle}{M_\chi^2}\frac{\mathrm{d}N_\gamma}{\mathrm{d}[E(1+z)]} \times \frac{1}{h(z)}\frac{\mathrm{d}n(z)}{\mathrm{d}M\mathrm{d}V}\int_0^{R_v}\rho_{\rm M}^2(r)\mathrm{d}^3r\,\mathrm{d}M\,\mathrm{d}z, \quad (8)$$

where c is the speed of light, $H_0 = 0.7$ is the present value of the Hubble constant and $h(z) = \sqrt{\Omega_{\rm M}(1+z)^3 + \Omega_\Lambda}$. We assume that $\Omega_{\rm M} = 0.27$ and $\Omega_\Lambda = 0.73$. We use an Einasto density profile parameter of $\alpha = 0.1645$, the value for the 'typical' halo mass formed from a 1σ peak in the mass–density field as given in Gao et al. (2008) (and we ignore any mass and redshift dependence of α). The quantity $\mathrm{d}N_\gamma/\mathrm{d}[E(1+z)]$ is the spectrum of the emitted photons at a source energy of $E(1+z)$, and the mass function of objects of mass M at redshift z is $\mathrm{d}n(z)/\mathrm{d}M\mathrm{d}V$. We use the mass function of Reed et al. (2007).

We assume that the annihilation proceeds to a $b\bar{b}$ quark final state, and that the distribution in the number of γ-rays emitted per source energy interval $E_{\rm s}$ are described by the functional form given in Bergstrom, Ullio & Buckley (1998), namely,

$$\frac{\mathrm{d}N}{\mathrm{d}E_{\rm s}} = \frac{1}{M_\chi}\left(\frac{E_{\rm s}}{M_\chi}\right)^{-3/2}\exp\left[-10.7\frac{E_{\rm s}}{M_\chi}\right]. \quad (9)$$

We estimate the cosmological γ-ray background for three different halo concentration distributions. First, we assume an Einasto functional form of the density as a function of radius and a one-to-one dependence of concentrations on mass and redshift as given in Maccio et al. (2007); this is case 'Einasto'. However, halo concentrations exhibit a distribution at fixed halo mass and redshift (see Section 4.1). As such, we consider a second case, 'Einasto + Gaussian', in which halo concentrations instead follow a Gaussian distribution, given by $\sigma_{\rm G} = 0.283c_{200}$, where c_{200} remains the Maccio et al. (2007) concentration as a function of mass and redshift, and the Einasto profile still describes the density distribution. This value for the Gaussian width corresponds to the fractional width found in our halo sample. Finally, we consider case 'Einasto + Lognormal' where the concentration distribution is lognormal about the mean concentration value, with dispersion given by $\sigma_{\rm LN} = 0.121$, and all other aspects of the background calculation (i.e. Einasto profile, mean concentration–mass–redshift relation) remain the same as the two other cases.

In Fig. 9, we show the expected cosmological γ-ray background for the three different distributions of dark matter. As expected, in the presence of a spread in the distribution of concentrations, the annihilation flux is increased relative to the case where there is a one-to-one mapping between concentration and mass. We find that a lognormal distribution would give rise to approximately a 10 per cent increase in the annihilation flux relative to our preferred Gaussian distribution of concentrations (which is only a few per cent higher than the simple case of no distribution in concentrations).

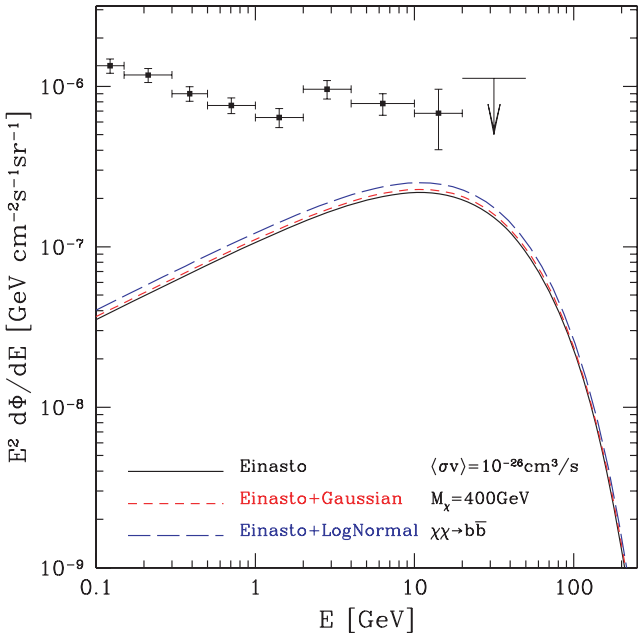

Figure 9. The effects of a Gaussian (short-dashed) and lognormal (long-dashed) distribution of concentration parameters to the cosmological extragalactic dark matter annihilation background. The *solid* curve represents the background computed by assigning a fixed $c(M)$ relationship without a spread. In all cases, the background is assumed to be due to a 400-GeV WIMP annihilating with a cross-section of 10^{-26} cm^3 s^{-1} into a $b\bar{b}$ quark pair. Data points are background measurements from the EGRET satellite (Strong, Moskalenko & Reimer 2004), which could include a contribution from dark matter annihilation.

5.3 The annihilation flux due to the smooth distribution of dark matter in the Milky Way

We now discuss the impact of the halo density PDF on the Milky Way annihilation flux along different lines of sight. The expected flux at a particular angle ψ with respect to the Galactic Centre depends on the distribution of dark matter densities along that line of sight. As that is an outcome of the particular concentration of the Galactic halo, drawn from a distribution of possible concentrations, there is a distribution of expected fluxes for each line of sight. Our calculations of the PDF of dark matter annihilation within the Milky Way assume that the PDF of the spherically averaged Galactic dark matter density and annihilation are well described by an Einasto profile and the corresponding PDF of halo concentrations, as we have shown to be the case for cluster-massed haloes.

The line-of-sight flux at an angle ψ with respect to the Galactic Centre can be written as

$$\frac{\mathrm{d}N_\gamma(\psi)}{\mathrm{d}E\mathrm{d}A\mathrm{d}t\mathrm{d}\Omega} = \frac{1}{4\pi}\frac{\langle\sigma v\rangle}{M_\chi^2}\frac{\mathrm{d}N_\gamma}{\mathrm{d}E}\int_0^{\ell_{\rm max}}\rho_{MW}^2[r(\ell,\psi)]\,\mathrm{d}\ell, \quad (10)$$

where $\ell_{\rm max} = \mathrm{d}_\odot[\cos\psi + \sqrt{(R_{MW}/\mathrm{d}_\odot)^2 - \sin^2\psi}]$ and $r = \sqrt{\mathrm{d}_\odot^2 + \ell^2 - 2\,\mathrm{d}_\odot\ell\cos\psi}$. We take the distance of the Sun from the Galactic Centre to be $\mathrm{d}_\odot = 8.5$ kpc (consistent with Gillessen et al. 2009), and the radius of the Milky Way halo $R_{200,\rm MW} = 250$ kpc, which implies $M_{200} = 1.8\times10^{12}\,\mathrm{M}_\odot$ and $M_{\rm vir} \simeq= 2.\times10^{12}\,\mathrm{M}_\odot$ (consistent with e.g. Guo et al. 2010). We assume an Einasto profile

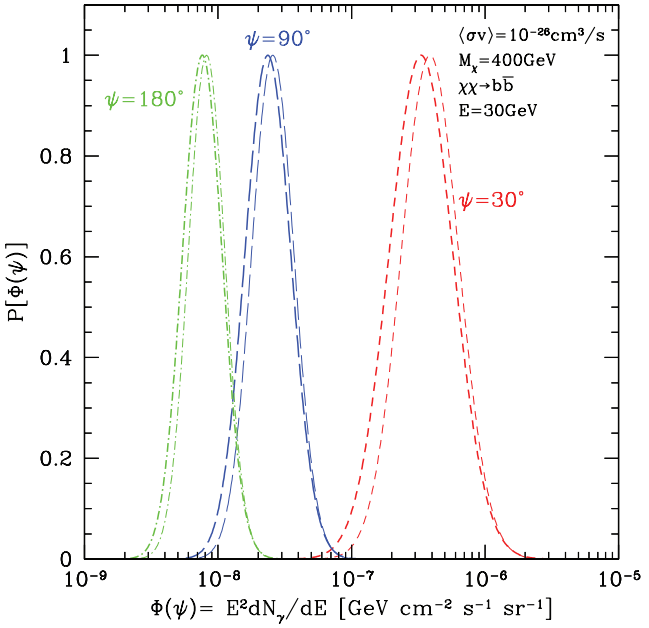

Figure 10. The PDF of γ-ray flux along a line of sight at 30° (short-dashed), 90° (long-dashed) and 180° (dot-dashed) degrees from the Galactic Centre for a Gaussian concentration distribution (thick curves) and a lognormal concentration distribution (thin curves). Note the smaller width of the distribution at high Galactic angles relative to the inner parts of the halo. Particle physics parameters are same as Fig. 9.

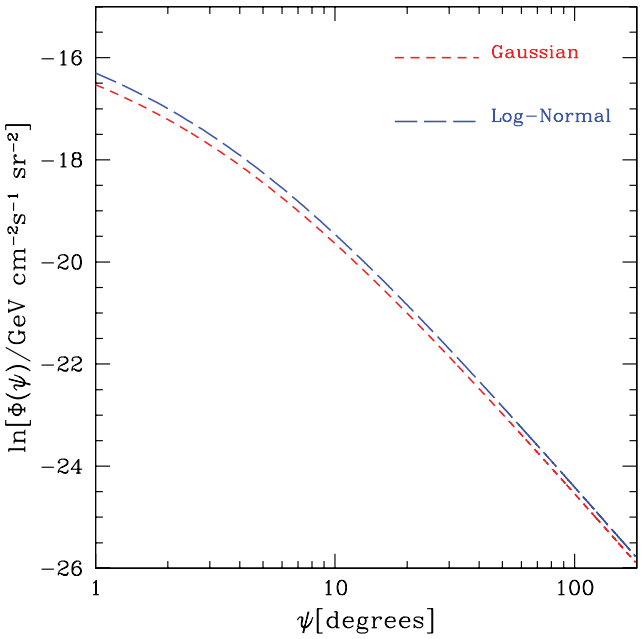

Figure 11. The dependence of the peak of the distributions (Gaussian/lognormal) to the angular distance of the line of sight with the Galactic Centre. Lognormal distribution in concentrations leads to a slightly higher peak in the flux PDF.

parameter $\alpha = 0.1645$, consistent with that for a halo of Milky Way mass (Gao et al. 2008).

In Fig. 10, we show the expected flux distribution at various angles with respect to the Galactic Centre computed using equation (10). We calculate the flux distribution for two cases, first where the distribution of concentrations is Gaussian, and secondly where the distribution of concentrations follows a lognormal distribution. We find that for a lognormal distribution of concentrations the width of the flux distribution along a line of sight is slightly narrower, while at the same time, the mean of the distribution is slightly higher. This is to be expected as the annihilation rate is sensitive to concentration parameter. The high concentration tail of the lognormal concentration distribution contributes to its higher mean flux, while the more extended low concentration range from the Gaussian distribution manifests itself into a broader distribution of fluxes at each particular angular Galactocentric distance.

It should also be emphasized that the shown distribution functions are uncorrelated, while in reality, because a single concentration must be defined for the halo, there are correlations between the flux at adjacent angular bins, and anticorrelations between angular values close to zero and 180°. A higher concentration halo has relatively more mass near the centre and less near the outer parts. Thus, highly concentrated haloes will have higher fluxes with respect to the distribution function towards the Galactic Centre, and will have relatively smaller fluxes towards the Galactic anticentre.

We now quantify the expected angular dependence of the peak and width of the flux PDF. The peak of the flux distribution is expected to be smaller at high angular distances from the Galactic Centre. This is a natural consequence of the centrally concentrated spherical distribution of dark matter in a halo, and enables a measure of the underlying density profile of the halo. In Fig. 11, we show the angular dependence of the peak flux. A good fit (within few per cent) to this function is obtained by a double power law as

$$\ln \bar{\Phi} = a_1 + a_2 \ln \psi + a_3 \ln(a_4 + \psi), \tag{11}$$

where the parameters a_1, a_2, a_3 and a_4 are given in Table 1. The width of the distribution is smaller at large angles from the Galactic Centre. This is to be expected because the effects of concentration are more apparent in the inner regions of the halo. At radial distances $r \gg r_{-2}$, the changes in the dark matter density due to different halo concentration values are smaller and therefore the flux distribution is narrower. In Fig. 12, we show the expected angular dependence of the width of the flux distribution. We find that a function of the form

$$\sigma = a_5 \ln \psi + a_6 \tag{12}$$

is a good (within few per cent) fit to the angular dependence of the width of the distribution function. The quantities a_5 and a_6 are given in Table 1. It is important to note here that for large radii ($r \gg r_{-2}$) the halo density PDF that we measured in Section 4.2 is larger than inferred from the concentration scatter, which implies that the values of flux uncertainty at large Galactocentric angles may be larger than our estimates. However, because the Solar Radius is well within r_{-2}, the flux should be dominated by the density distribution within r_{-2}, even towards the Galactic anticentre, so effects of large radii scatter on the flux PDF should be small.

Table 1. Fitting parameters of equations (11) and (12) for the peak and width of the γ-ray annihilation flux distribution function along a Galactic line of sight.

	a_1	a_2	a_3	a_4	a_5	a_6
Gaussian	−13.70	−0.39	−1.95	3.27	−0.12	0.98
Lognormal	−13.48	−0.40	−1.96	3.22	−0.11	0.87

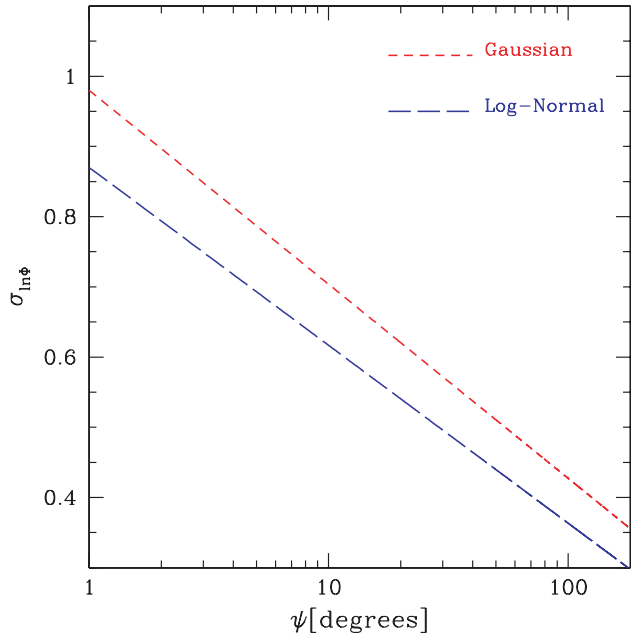

Figure 12. The dependence of the width of the distributions (Gaussian/lognormal) to the angular distance of the line of sight with the Galactic Centre. Lognormal distribution in concentrations leads to a slightly narrower flux PDF.

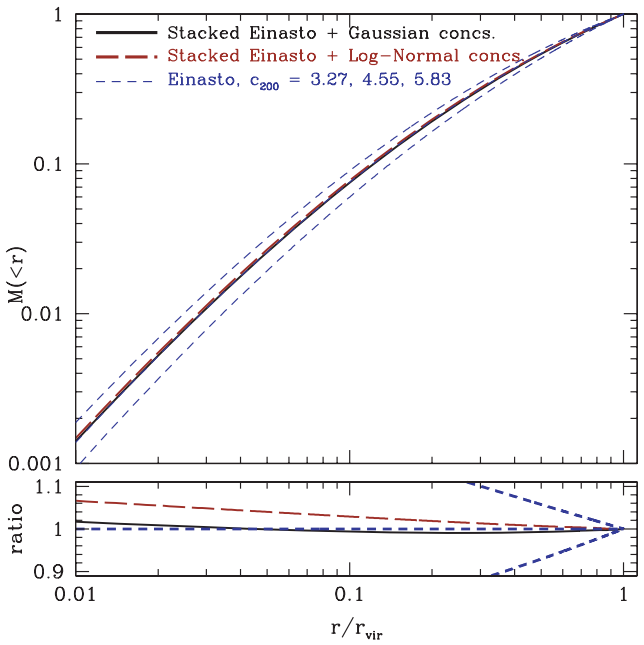

Figure 13. Enclosed mass in spherical shells for mock stacked halo samples with Einasto profile at $c_{200} = 4.55$ plus Gaussian concentration distribution and lognormal concentration distribution. $c_{200} = 3.27$ and $c_{200} = 5.83$ denote the 1σ range in concentration distribution. Bottom panel shows the ratio of each mass profile with respect to mean concentration, $c_{200} = 4.55$, Einasto profile. Level of agreement with mean concentration indicates robustness of $M < r$ in stacked halo samples against bias caused by halo-to-halo scatter in concentrations.

5.4 Other applications

5.4.1 Cosmological uncertainty of the local dark matter density

Applying our results, as before, to a Milky Way mass of $M_{200} = 1.8 \times 10^{12}\,\mathrm{M}_\odot$, with an ($\alpha = 0.1645$) Einasto profile of concentration of $c_{200} = 5.97$ (using the concentration–mass relation of Maccio et al. 2008), and a Solar radius of 8.5 kpc implies a Solar radius total matter density of $0.210^{+0.42}_{-0.45}\,\mathrm{GeV\,cm^{-3}}$ if the concentration PDF is assumed to be Gaussian with width proportional to our values of $\sigma_c/c = 0.283$. Assumptions of a lognormal distribution of width $\sigma_{\mathrm{LN}} = 0.121$ results in only minor changes for a local density range of $0.210^{+0.047}_{-0.039}\,\mathrm{GeV\,cm^{-3}}$, which can be compared with several observational estimates. Bergstrom et al. (1998) find an allowed range of [0.2–0.8] $\mathrm{GeV\,cm^{-3}}$, and a more recent work by Weber & de Boer (2010) find an acceptable range of [0.2–0.4] $\mathrm{GeV\,cm^{-3}}$. However, tighter constraints are found by Widrow, Pym & Dubinski (2008) and Catena & Ullio (2010), who utilize a variety of dynamical observables to estimate, respectively, $0.304 \pm 0.053\,\mathrm{GeV\,cm^{-3}}$ and $0.385 \pm 0.027\,\mathrm{GeV\,cm^{-3}}$ for the dark matter density. These estimates are somewhat larger than our cosmological range, which hints at the possibility that the Solar radius dark matter density has been enhanced by 'adiabatic contraction' in response to baryon cooling.

5.4.2 Implications for halo stacking

Our results have implications for many astrophysical applications that depend upon the mass distribution within haloes. One such example is the technique of 'stacking'haloes to improve signal-to-noise ratio, commonly employed in simulations and observations. In one such application, large numbers of simulated halo density profiles are stacked to measure the mean density profile to high precision (e.g. Gao et al. 2008; Hayashi & White 2008). From an observational perspective, stacking many haloes of similar mass greatly reduces the noise in, for example, weak lensing determinations of halo mass profiles and concentrations (e.g. Mandelbaum, Seljak & Hirata 2008; Sheldon et al. 2009a, b; Mandelbaum et al. 2010).

Our results support the viability of halo 'stacking'. Due to the fact that the distribution of densities at fixed radius is Gaussian and the distribution of concentrations is also Gaussian, a stacked density profile is indeed an accurate representation of the median profile. This is particularly convenient in that it allows the mean halo profile to be parameterized into an analytic form without bias, and allows unbiased stacking of observational mass profiles. In Fig. 13, we have verified that the cumulative cluster mass distribution also remains unbiased. We compare the Einasto form of a three-dimensional enclosed mass profile of $c_{200} = 4.55$ and $\alpha = 0.19$ with the same quantity for a mock stacked halo drawn from a Gaussian distribution of concentrations of mean $c_{200} = 4.55$ and scatter $\sigma_{\mathrm{G}} = 0.283 c_{200}$, and find agreement to better than 1 per cent, except within a few per cent $\mathrm{r_{vir}}$ where differences approach 2 per cent. This implies that mass profiles determined by lensing studies should be free from biases associated with halo stacking. Cosmological simulations have been used to demonstrate that accurate three-dimensional mass profiles can be constructed from stacked shear signals (e.g. Johnston et al. 2007); our work shows that any potential systematic bias related to the distribution of halo concentrations or densities will be negligible for a Gaussian concentration PDF, even for future precision surveys. If, instead, the density distribution had been lognormal, then a stacked halo would have been biased towards higher cumulative masses at small radii, by more than 6 per cent at 1 per cent r_{vir} in our test case.

6 LIMITATIONS OF THIS WORK

In this work, we do not consider other potential important factors to the annihilation rate, which could possibly be dominant over the halo-to-halo scatter associated with hierarchical structure formation (via the distribution of concentrations) that we have examined. Among them is the amount of substructure in small subhaloes and streams (the 'clumpy' dark matter component), whose contribution can boost the annihilation rate relative to that of a smooth halo, and will add to the uncertainty in the local dark matter density (e.g. Kamionkowski & Koushiappas 2008; Vogelsberger et al. 2009; Kamionkowski, Koushiappas & Kuhlen 2010). We also ignore any gravitational coupling that the differential evolution of baryonic halo component may have on the dark matter halo structure. Baryon influences may include gas cooling; this could cause the dark matter halo to respond to the deeper potential by 'adiabatic contraction' (Blumenthal et al. 1986). However, strong stellar or AGN feedback could instead lead to shallowing of the dark matter potential (e.g. Duffy et al. 2010). Although these effects may be important, they are beyond the scope of this study.

Our measurements of the cosmological distribution of halo concentrations, densities and other quantities utilized only clusters from the simulation (because those are the best resolved haloes). Our application towards annihilation rates in the Galaxy relies upon the assumption that the behaviour of the halo-to-halo profile scatter is similar for galaxies and clusters, namely that the probability distribution of the mean density in radial shells is always described by the Einasto profile with a Gaussian distribution in halo concentrations. The assertion that the distribution of halo concentration remains universally Gaussian, while speculative, is supported by the fact that the logarithmic width and shape of the concentration distribution has weak or no mass or redshift dependence (e.g. Bullock et al. 2001; Maccio et al. 2007; Neto et al. 2007; Gao et al. 2008). This is expected from the self-similar scatter in formation time with mass and the close correlation between formation time and concentration (Wechsler et al. 2002). Additionally, Knollmann et al. (2008) used scale-free simulations to show that the scatter in halo profile concentration and density slope has little dependence on matter power spectral index (which varies with halo mass) over a range bracketing well beyond the effective spectral indices of clusters and galaxies. Future studies are warranted utilizing a wider range in halo masses to determine whether the distribution of concentrations is universally Gaussian.

7 CONCLUSIONS

The PDF of dark matter within haloes, as we have explored in this work, provides some basis for interpreting both indirect and direct dark matter detection experiments in a cosmological context. Constraints upon the dark matter density, particle mass or the self-annihilation cross-section depend on the PDF of dark matter.

Our results indicate that halo concentration is the primary cosmological contributor to the dark matter PDF. This implies a particular correlation between the local dark matter density, relevant for direct detection efforts, and the dark matter density in the direction of the Galactic Centre (and elsewhere), applicable to indirect detection experiments. The effect of halo concentration should thus be a crucial factor in verifying the consistency of dark matter density constraints made from multiple dark matter detection techniques. Ultimately, dark matter signals might be able to test the validity of the ΛCDM cosmological model through estimates of the dark density at differing locations within the Milky Way halo, and perhaps also within other haloes.

ACKNOWLEDGMENTS

This work was partially supported by the DOE through the IGPP, the LDRD-DR and the LDRD-ER programmes at LANL. We thank Carlos Frenk, Tom Theuns, Salman Habib, Katrin Heitmann, and Zarija Lukić for helpful discussions. DR thanks KITP for its hospitality where portions of this work were completed. LG acknowledges support from the one-hundred-talents programme of the Chinese academy of science (CAS), the National basic research programme of China (programme 973 under grant No. 2009CB24901), NSFC grants (Nos. 10973018) and an STFC Advanced Fellowship, as well as the hospitality of the Institute for Computational Cosmology in Durham, UK. We thank the Virgo Consortium for kindly allowing us use of the Millennium Simulation. We are grateful to the anonymous referee for insightful suggestions.

REFERENCES

Bergstrom L., Ullio P., Buckley J., 1998, Astropart. Phys., 9, 137
Bertone G., Hooper D., Silk J., 2005, Phys. Rept., 405, 279
Blumenthal G., Faber S., Flores R., Primack J., 1986, ApJ, 301, 27
Bullock J. S., Kolatt T. S., Sigad Y., Somerville R. S., Kravtsov A. V., Klypin A. A., Primack J. R., Dekel A., 2001, MNRAS, 321, 559
Catena R., Ullio P., 2010, J. Cosmol. Astropart. Phys., 08, 004
Duffy A., Schaye J., Kay S., Dalla Vecchia C., 2008, MNRAS, 390, L64
Duffy A., Schaye J., Kay S., Dalla Vecchia C., Booth C., 2010, MNRAS, 405, 2161
Einasto J., 1965, Trudy Inst. Astrofiz. Alma-Ata, 51, 87
Eke V., Cole S., Frenk C., 1996, MNRAS, 282, 263
Fukushige T., Kawai A., Makino J., 2004, ApJ, 606, 625
Gao L., White S. D. M., 2006, MNRAS, 373, 65
Gao L., Navarro J., Cole S., Frenk C. S., White S. D. M., Springel V., Jenkins A., Neto A., 2008, MNRAS, 387, 536
Gillessen S., Eisenhauer F., Trippe S., Alexander T., Genzel R., Martins F., Ott T., 2009, ApJ, 692, 1075
Guo Q., White S., Li C., Boylan-Kolchin M., 2010, MNRAS, 404, 1111
Hayashi E., White S. D. M., 2008, MNRAS, 388, 2
Jing Y., 2000, ApJ, 535, 30
Johnston D., Sheldon E., Tasitsiomi A., Frieman J., Wechsler R., McKay T., 2007, ApJ, 656, 27
Jungman G., Kamionkowski M., Griest K., 1996, Phys. Rep., 267, 195
Kamionkowski M., Koushiappas S. M., 2008, Phys Rev D, 77, 10, 3509
Kamionkowski M., Koushiappas S. M., Kuhlen M., 2010, Phys Rev D, 81, 043532
Knollmanns S., Power C., Knebe A., 2008, MNRAS, 385, 545
Kuhlen M., Diemand J., Madau P., 2008, ApJ, 686, 262
Lukić Z., Reed D., Habib S., Heitmann K., 2009, ApJ, 692, 217
Maccio A., Dutton A., van den Bosch F., Moore B., Potter D., Stadel J., 2007, MNRAS, 378, 55
Maccio A., Dutton A., van den Bosch F., 2008, MNRAS, 391, 1940
Mandelbaum R., Seljak U., Hirata C., 2008, J. Cosmol. Astropart. Phys., 8, 6
Mandelbaum R., Seljak U., Baldauf T., Smith R., 2010, MNRAS, 405, 2078
Moore B., Governato F., Quinn T., Stadel J., Lake G., 1998, AJ, 499, L5
Navarro J. F., Frenk C. S., White S. D. M., 1996, ApJ, 462, 563 (NFW)
Navarro J. F., Frenk C. S., White S. D. M., 1997, ApJ, 490, 493 (NFW)
Navarro J. F. et al., 2004, MNRAS, 349, 1039
Neto A. et al., 2007, MNRAS, 381, 1450
Power C., Navarro J. F., Jenkins A., Frenk C. S., White S. D. M., Springel V., Stadel J., Quinn T., 2003, MNRAS, 338, 14
Reed, D., Governato F., Verde L., Gardner J., Quinn T., Merritt D., Stadel J., Lake G., 2005, MNRAS, 357, 82

Reed D. S., Bower R., Frenk C. S., Jenkins A., Theuns T., 2007, MNRAS, 374, 2
Seljak U., Zaldarriaga M., 1996, ApJ, 469, 437
Sheldon E. et al., 2009a, ApJ, 703, 2217
Sheldon E. et al., 2009b, ApJ, 703, 2232
Springel V., 2005, MNRAS, 364, 1105
Springel V. et al., 2005, Nat, 435, 629
Springel V. et al., 2008, MNRAS, 391, 1685
Springel V. et al., 2008, Nat, 456, 73
Strong A., Moskalenko I., Reimer O., 2004, ApJ, 613, 956
Ullio P., Bergstrom L., Edsjo J., Lacey C., 2002, Phys. Rev. D, 66, 123502
Vogelsberger M. et al., 2009, MNRAS, 395, 797
Weber M., de Boer W., 2010, A&A, 509, 25
Wechsler R. H., Bullock J. S., Primack J. R., Kravtsov A. V., Dekel A., 2002, ApJ, 568, 52
Widrow L., Pym B., Dubinski J., 2008, ApJ, 679, 1239
Zavala J., Springel V., Boylan-Kolchin M., 2010, MNRAS, 405, 593

This paper has been typeset from a TEX/LATEX file prepared by the author.